Thermoelectric energy recovery at ionic-liquid/electrode interface

Marco Bonetti, Sawako Nakamae, Bo Tao Huang, Thomas J. Salez, Cécile Wiertel-Gasquet, Michel Roger

▶ **To cite this version:**

HAL Id: cea-01366727

https://hal-cea.archives-ouvertes.fr/cea-01366727

Submitted on 15 Sep 2016

Thermoelectric energy recovery at ionic-liquid/electrode interface

Marco Bonetti,[1] Sawako Nakamae,[1] Bo Tao Huang,[1] Thomas J. Salez,[2, 1] Cécile Wiertel-Gasquet,[1] and Michel Roger[1]

[1]*Service de Physique de l'Etat Condensé, CEA-IRAMIS-SPEC, CNRS-UMR 3680, CEA Saclay, F-91191 Gif-sur-Yvette Cedex, France*

[2]*École des Ponts ParisTech, 6 et 8 avenue Blaise Pascal, Champs-sur-Marne F-77455 Marne-la-Vallée, France*

(Dated: (23 June 2015))

A Thermally Chargeable Capacitor containing a binary solution of 1-ethyl-3-methylimidazolium bis(trifluoromethylsulfonyl)-imide (EMIMTFSI) in acetonitrile is electrically charged by applying a temperature gradient to two ideally polarisable electrodes. The corresponding thermoelectric coefficient is -1.7 mV/K for platinum foil electrodes and -0.3 mV/K for nanoporous carbon electrodes. Stored electrical energy is extracted by discharging the capacitor through a resistor. The measured capacitance of the electrode/ionic-liquid interface is 5 μF for each platinum electrode while it becomes four orders of magnitude larger $\approx$ 36 mF for a single nanoporous carbon electrode. Reproducibility of the effect through repeated charging-discharging cycles under a steady-state temperature gradient demonstrates the robustness of the electrical charging process at the liquid/electrode interface. The acceleration of the charging by convective flows is also observed. This offers the possibility to convert waste-heat into electric energy without exchanging electrons between ions and electrodes, in contrast to what occurs in most thermogalvanic cells.

I. INTRODUCTION

Conversion of low-grade waste heat (typically at temperatures $< 200^o$ C) into electrical energy has become a topical challenge in energy research of the 21st century. For example, solid state thermoelectric converters are attracting attention as promising devices for portable generators.[1] An alternative to solid-state thermoelectric generators can be found in thermogalvanic cells containing an electrolyte and a redox couple[2–15] where the difference in the redox potentials (reaction entropies) at two electrodes under a thermal gradient can be used to generate electricity. In thermogalvanic cells, ions circulate inside the cell and exchange electrons with the electrodes. Presently, high thermogalvanic coefficient values are found in ionic-liquid/organic solvent mixtures[16] using various inorganic and organic redox couples.[9–11] The redox reaction can also take place inside electrodes via insertion/deintercalation of ions, *e.g.* lithium in an intercalated compound like $Li_xV_2O_5$, leading to a thermally rechargeable battery.[17]

It has recently been proven by Qiao's group[18–21] that the thermocells can also be conceived with pure electrolytes (without redox couples) that operate with *ideally polarizable* electrodes with no exchange of electrons between electrodes and the electrolyte ions. In their experiments, platinum and nanoporous carbon electrodes were immersed in a cell made of two compartments maintained at different temperatures and electrically connected through a salt bridge. In this case, no electrical current flows inside the cell and thus the thermocell operates by a pure capacitive process at the electrodes. Therefore the cell operates as a *"Thermally Chargeable Capacitor"* (TCC). The thermoelectric potential is then due to the internal electric field[22] generated by the thermal drift of ions (Soret effect) in the electrolyte and the temperature dependence of the surface potential at the liquid/electrode interfaces. At the contact with electrodes, ions lose a part of their solvation layers and their entropy is modified. The corresponding thermoelectric potentials for aqueous solutions of alkaline salts have been compared in Ref. 20. The electrical energy stored in the form of accumulated charge at the electrode interfaces can be subsequently recovered by 'discharging' through an external load.

In this paper, we extend the work of Qiao's group[20,21] to the interface between *ideally polarisable* electrodes and an ionic liquid. Ionic liquids (IL) have a low melting temperature close to room temperature unlike most molten salts, a relatively high decomposition temperature[16,23] and a large electrochemical window.[24] They can operate on a wide temperature range 0–200°C, suitable for low-grade waste heat recovery applications.

The IL/metal electrodes interface is known to be complex, extending over 4–8 layers, giving rise to a vast literature (for a short review on this subject see *e.g.* Ref. 25). IL's large ions can be adsorbed on a metal surface in multiple configurations.[26] Such conformational changes are accompanied by a partial loss of entropy from the bulk state, possibly resulting in a large temperature-dependent surface potential. Here, we have chosen the binary mixture 1-ethyl-3-methylimidazolium bis(trifluoromethylsulfonyl)-imide (EMIMTFSI, 391.3 g/mole), diluted to 2M in acetonitrile (AN). This concentration gives a weak maximum of the Seebeck coefficient and the highest ionic conductivity $\sigma(40^o C)= (57.3\pm0.5)$ mS cm^{-1} among different organic solvents.[27]

To estimate the electrical energy stored in the TCC under a temperature gradient, we have performed discharge potential measurements by connecting the electrodes to an external resistive load. Bare platinum foil electrodes were first used as a model system which has
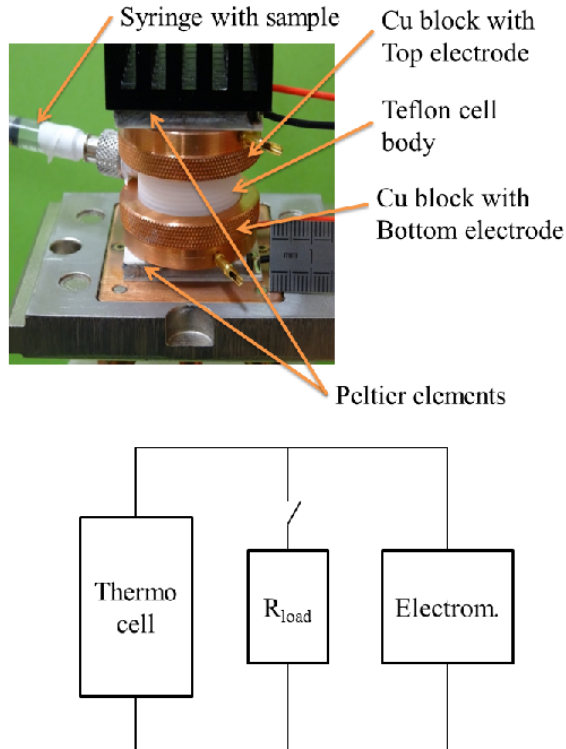
FIG. 1. Top:Thermally Chargeable Capacitor. Two copper blocks screwed onto the Teflon cell body press the platinum foil electrodes against two O-rings to achieve sealing. The copper blocks are electrically in contact with the electrodes and are thermally regulated by means of Peltier elements. The electrodes are connected to an electrometer for open-circuit potential measurement, or to a resistive load via a switch-box to discharge the cell. The cell is 25 mm in height and 35 mm in diameter. Notice the syringe that is used to fill the cell and allows the fluid to expand when the cell is heated. Bottom: corresponding electrical circuit (see text for explanations).

been extensively studied both experimentally and theoretically. Repeated cycles of charge/discharge under a constant temperature gradient show that the charging of the IL/electrode interface layer is a robust process. The same experiments were then repeated with platinum-foil electrodes covered with a thin sheet of nanoporous carbon, which increases the electrode capacitance by four orders of magnitude, a necessary condition for heat to electrical energy conversion applications.

II. EXPERIMENTAL SETUP

The experimental setup (TCC geometry) is different from that of Lim *et al.*[20] Rather than two horizontally connected compartments held at different temperatures, here the differential potential measurements were carried

out in a single-volume vertical cell with a $\phi = 6$ mm diameter sample cavity machined out from a solid Teflon cylinder closed by two symmetrical 10 mm diameter platinum foil electrodes of 100 μm thickness (99.99 % pure, Sigma-Aldrich). (A complete view of the cell assembly is shown in Figure 1.). Our geometry is thus similar to that corresponding to usual supercapacitors. The Pt electrode surface is wet polished with a diamond paste with particle sizes reduced from 9 to 1 μm, subsequently cleaned in an ultrasonic bath with acetone or acetonitrile and rinsed in ultrapure water and then vacuum dried. Additional cleaning by immersion of the electrodes in a concentrated HCl (36%wt) solution for many hours and ultrasonication in ultrapure water did not have any effect on the measured thermoelectric potential. The electrode surface in contact with the liquid is $A \approx 0.28$ cm^2 and the distance between the electrodes is $l = 6$ mm. Two 10 mm thick copper blocks are screwed onto the cell body, thereby squeezing the Pt electrodes hermetically against the Teflon cylinder (the sample volume is 0.17 cm^3). To investigate the influence of the effective electrode surface, a thin sheet of nanoporous carbon (NanoTuneX Y-Carbon) with $\approx$20 nm average pore diameter was sandwiched between the platinum foil and the cell body. The electrodes are electrically and thermally in contact with the top and bottom copper blocks which ensures a fast heat transfer to and from the liquid mixture. The temperature of the Cu blocks is monitored by 100 Ω-platinum resistance thermometers and regulated by a temperature controller (LakeShore 340) that finely adjusts the output power of two Peltier elements with lapped alumina surface of 30x30 mm^2. The thermal stability of both Cu blocks, δT, is less than 2 mK over many hours. The natural convection of the liquid mixture can be either minimized; by heating only the top Cu-block while keeping the bottom Cu-block at 30 ^{o}C, or maximized; by reversing the heating direction. The maximum allowed temperature difference is $\approx 60^o$C, corresponding to a temperature gradient across the cell body ≈ 65 K cm^{-1}. The sample liquid filling is achieved by injection through a small radial hole in the cylindrical cavity using a syringe. The syringe is left in place so that overfilling of the cell when the two Cu blocks are screwed together or the thermal expansion of the fluid during the measurements is compensated by the displacement of the piston inside the syringe. The electric conductivity of the sample was also measured using the same cell. The ionic liquid (EMIMTFSI, 98% purity, Sigma-Aldrich) and acetonitrile (99.8% purity, Sigma-Aldrich) were used as received without further purification. The TCC is filled with a solution of 2M EMIMTFSI in AN. The water content was less than 0.05% w/w (Karl-Fisher).

The entire cell is electrically floating with respect to the Peltier elements and is placed in a Faraday cage. The thermoelectric open-circuit potential (during charging) and the discharge potential between the electrodes are measured by a high impedance electrometer with a 10^{14} Ω input resistance (Keithley K-6514). Discharging

is achieved via a manual switch that connects instantaneously the cell electrodes to an external resistive load that ranges between 1.5 kΩ to 100 MΩ. The electrical circuit corresponding to the measurement setup is presented in Figure 1 (bottom panel).

III. EXPERIMENTAL RESULTS WITH PLATINUM-FOIL ELECTRODES

III.1. Thermoelectric coefficient

The open circuit potential ΔV between the hot and cold electrodes (no current flow) is proportional to the temperature difference ΔT between the two electrodes:

$$\Delta V = -\Lambda \Delta T. \tag{1}$$

Λ represents the *thermoelectric coefficient*. ΔV can be split into three contributions:

$$\Delta V = \phi_H - E_{int}l - \phi_C \tag{2}$$

where ϕ_H and ϕ_C represent the interface electrostatic potentials at the hot and cold electrodes, l is the electrode separation and E_{int} is a uniform Seebeck internal electric field resulting from the thermal drift of ions:

$$\mathbf{E}_{int} = S_e \nabla T. \tag{3}$$

S_e represents the Seebeck coefficient. ϕ_H and ϕ_C are the results of IL anions and cations adsorbed at the metal interfaces. Such adsorption effects have been observed by scanning tunelling microscopy,[26,28] atomic force microscopy,[29] angle-resolved X-ray photoelectron spectroscopy,[30] electrochemical impedance spectroscopy.[31,32] The temperature dependence of the structure of an IL/metal interface has also been evidenced in Ref. 29, 31, and 32, which implies that the interface potential ϕ depends on temperature as well. For small temperature variations, we can write:

$$\phi_H - \phi_C = \frac{d\phi}{dT}\Delta T \tag{4}$$

and we have:

$$\Lambda = S_e - \frac{d\phi}{dT} \tag{5}$$

We expect the second term in Eq. (5) to be particularly important in the case of large-ion adsorption since $d\phi/dT$ depends on $\Delta S_{conf}/e$, where ΔS_{conf} is the change in configurational entropy of adsorbed ions.[22,40]

For monovalent ions, the Seebeck coefficient of an electrolyte at initial state, *i.e.* when a temperature gradient is applied while the ion concentration is still uniform throughout the cell, is:[22]

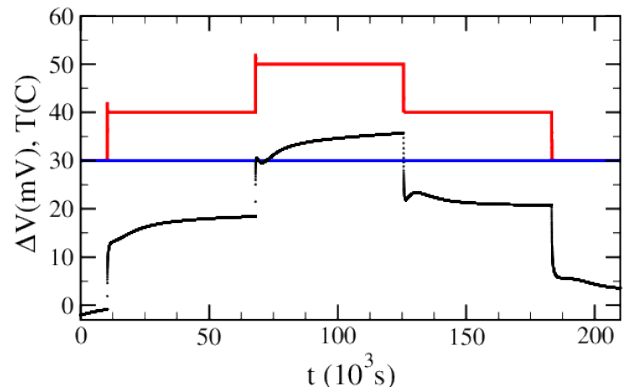$$S_e^{init} = (t_+ \widehat{S}^+ - t_- \widehat{S}^-)/e \tag{6}$$

FIG. 2. Thermoelectric potential ΔV (black line) for a solution of EMIMTFSI (2M) in acetonitrile when the temperature of the top electrode (red line) is changed by a 10 ^{o}C step between 30°C and 50°C. The temperature of the bottom electrode (blue line) is maintained at 30°C.

where $\widehat{S}^+$, $\widehat{S}^-$ are the Eastman entropies of transfer of cations and anions and t_+, t_- the corresponding Hittorf transport numbers. When ions have moved to establish a Soret steady-state, in an open circuit condition, we have:[22,33]

$$S_e^{st} = (\widehat{S}^+ - \widehat{S}^-)/(2e) \tag{7}$$

A typical time evolution of ΔV when the temperature of the hot electrode is heated from 30°C to 50°C by 10°C steps, while the cold electrode is maintained at 30°C is shown in Figure 2. A nice reversibility is observed when cooling the hot electrode back to 30°C. An average value $\Lambda_{Pt} \approx -1.7$ mV K^{-1} is deduced from the measurement. The time evolution of ΔV corresponding to the first heating cycle is zoomed in Figure 3. This evolution is governed by the Soret diffusion of IL ions through the cell which, in one dimension, leads to:[34,35]

$$\Delta V(t) - \Delta V(0) = (\Delta V(\infty) - \Delta V(0)) \times$$
$$\left[1 - \frac{8}{\pi^2} \sum_{n \text{ odd}} \frac{\exp(-n^2 t/\theta)}{n^2}\right] \tag{8}$$

where $\theta = l^2/(\pi^2 D)$ is the characteristic time of diffusion with D representing the diffusion coefficient of cations. For $t > \theta$ only the lowest order term in the sum of exponential terms is significant.

The experimental data at $t > 10000$ s (Figure 3) have been fit to Eq. (8). An additional linear term corresponding to an instrumental drift of 74 μV/hour was also taken in account. The characteristic time θ is ≈ 10620 s $\approx$ 3 hours from which we estimate $D \approx 3.4 \times 10^{-10}$ m^2 s^{-1}. This value is three times higher than the value deduced from nuclear magnetic resonance measurements in pure EMIMTFSI at room temperature.[36] Such an increase in D is in agreement with the numerical simulations[37] that predict a 4-fold boost in the diffusion coefficient of 2M EMIMBF4 diluted in acetonitrile. In Figure 3, the red dashed line represents the extrapolation of the *full*

Eq. (8) down to $t = 0$. Note that the time required for the onset of a uniform temperature gradient is 5 to 10 mn, which explains the deviation from Eq. (8) at $t < 1000$ s.

III.2. TCC charging and discharging

Discharging of the TCC is obtained by connecting the two electrodes to an external resistive load (R$\approx$ 6–100 MΩ) much larger than the internal resistance of the liquid sample (37 Ω at 40°C). The experimental procedure for charging/discharging measurements is described as follows:

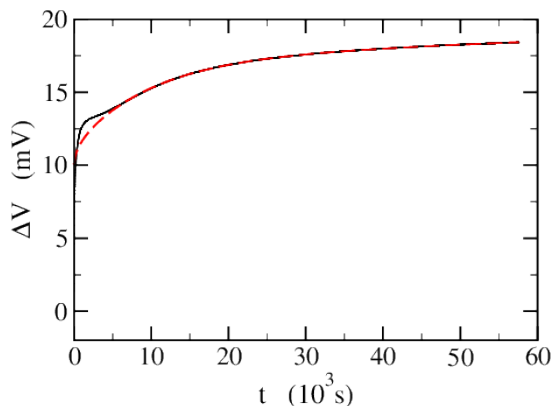1. Initial discharge: The cell is completely discharged

FIG. 3. Zoom on the first step in Figure 2 (solid black line). The red dashed line is a fit through Eq. (8).
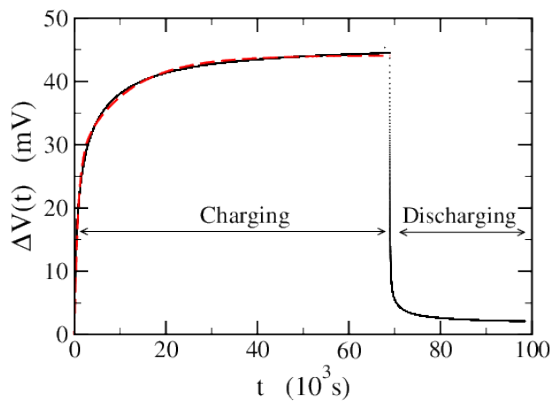

FIG. 4. Charge/discharge potential of the TCC with Pt foil electrodes as a function of time. At time $t = 0$, the TCC is completely discharged and charging potential is measured in open circuit (cell connected to the electrometer alone) during 19 hours up to a steady-state value. Discharged is then accomplished by connecting the electrodes to a 20 MΩ resistor. During the whole process the top and bottom electrode are maintained at 50°C and 30°C respectively. The dashed red line is fit to a sum of two exponentials with characteristic times $\alpha = 790$ s and $\theta = 10600$ s.

through a low value resistor.

2. Charging phase: At an experimentally defined $t = 0$, the cell is put in open circuit (disconnected from the resistive load). From $t = 0$ to $t \approx 19$ hours we observe an increase of the open-circuit potential ΔV from 0 to a steady value of ≈ 45 mV (see Figure 4, charging phase). At this stage, the TCC is considered to be fully charged. $\Delta V(t)$ can be fit by the sum of two exponential terms with characteristic times $\alpha = 790$ s ≈ 13 min and $\theta = 10600$ s ≈ 3 hours. θ is close to the time-scale corresponding to the ion diffusion through the cell (see previous subsection).

3. Discharging phase: The electrodes are then connected to an external resistive load (20 MΩ for the measurement shown in Figure 4). The potential ΔV drops rapidly to a low value ≈ 2 mV.

Note that a steady-state temperature gradient between the top (50°C) and the bottom (30°C) electrode is maintained throughout the measurements.

Similar charge/discharge curves are obtained with the resistive loads $R = 6.4$, 42 and 100 MΩ. The discharge potentials are reported in a semi-log plot in Figure 5. As can be seen from the figure, the semi-logarithmic plots of $\ln \Delta V(t)$ are not linear, thus a rational fraction containing two time constants was used to fit the data. The time constants τ and θ characterize respectively the fast (discharging) and slow (thermodiffusion) processes:

$$-\frac{t + at^2 + bt^3}{\tau + ct + \theta bt^2} \quad (9)$$

The long time-scale constant $\theta \approx 3\pm1$ hours is roughly independent of the resistive load. It is comparable to the diffusion time of ions through the cell and may be due
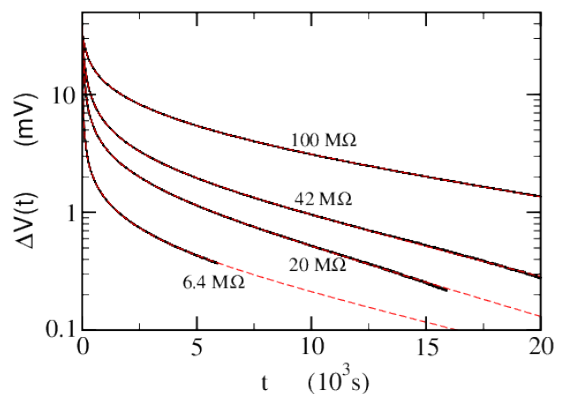

FIG. 5. Discharge potential through different loads from 6.4 to 100 MΩ. Solid black lines: experimental data. Red dashed lines: fits using Eq. (9). TCC with Pt-foil electrodes, filled with EMIMTFSI (2M) in acetonitrile. A small instrumental offset at large t has been subtracted from the experimental data.
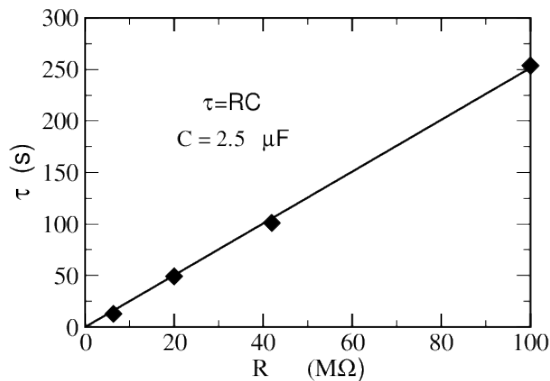
FIG. 6. Short relaxation time τ corresponding to different resistive loads $R = 6.4, 20, 42$ and 100 MΩ.

to the readjustment of the ion concentration gradient in the bulk to satisfy the new steady-state boundary conditions corresponding to equipotential electrodes rather than open-circuit potential electrodes.

The corresponding values of the short relaxation time τ are reported as a function of the load resistance R in Figure 6. As seen from the graph, τ is proportional to R, from which one can extract capacitance $C = \tau/R \approx 2.5$ μF. Assuming identical electrodes, this corresponds to the capacitance of two electrode/ionic-liquid interfaces in series (see section IV). The capacitance of a single electrode is thus $C_{Pt} = 5$ μF, giving per surface area $C_{Pt}/A = 18\mu$F/cm^2. This value is of the same order of magnitude as the differential capacitance obtained through electrochemical impedance spectroscopy at the interface of similar ILs with noble-metal electrodes, $e.g.$ ≈ 4 μFcm^{-2} with 1-butyl-3-methylimidazolium hexafluorophosphate (BMIMPF6) on platinum electrodes,[31] and $\approx 6 - 8$ μFcm^{-2} with 1-ethyl-3-methylimidazolium tris(pentafluoroethyl)-trifluorophosphate (EMIMFAP) on gold electrodes.[38] This indicates that the short relaxation time τ is indeed related to the fast rearrangement of the ions at the liquid/solid interface, while negligible current flows through the bulk sample.

From the discharge potential the current flowing through the resistive load can be calculated. The time integration of the electric current gives an estimate on the total charge Q accumulated in the electrodes. Figure 7 shows an almost constant value of the charge $Q \approx 1$ μC for all R, corresponding to a charge density (Q/A) of ≈ 3 μC cm^{-2}.

III.3. Charge/Discharge cycling at constant temperature gradient

To test the recharging capability of the TCC, we have performed many charge/discharge cycles with progressively increasing charging time t_{ch} under a steady-state

temperature gradient (see Figure 8). A 20 MΩ resistive load was used for discharging. Here, we have intentionally stopped charging/discharging before reaching the stationary states. Figure 9 shows the normalized differential potential $\Delta V/\Delta V_0$ as a function of t_{ch}, where ΔV_0 is the stationary differential potential measured when the electric layer is fully charged. Two sets of data are represented. The circles are obtained for pure diffusive heat flow when the temperature of the top electrode is heated to 50°C and the bottom is maintained close to room temperature (30°C). The triangles are obtained when an internal convective flow settles in the cell heated from the bottom with the same temperature difference.

When heated from the bottom, the onset of convective flow occurs at a critical Rayleigh number $Ra_c \approx 1700$.[39]
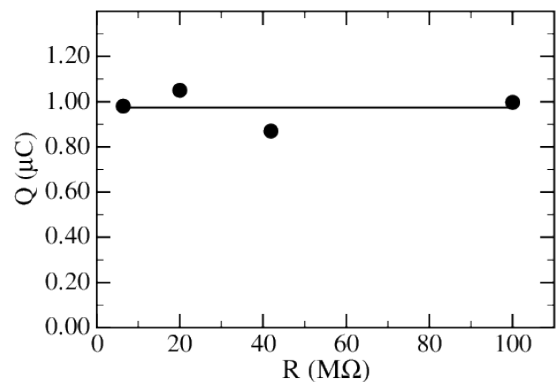

FIG. 7. Charge Q accumulated in the IL/Pt-electrode interface as a function of the resistive load R.
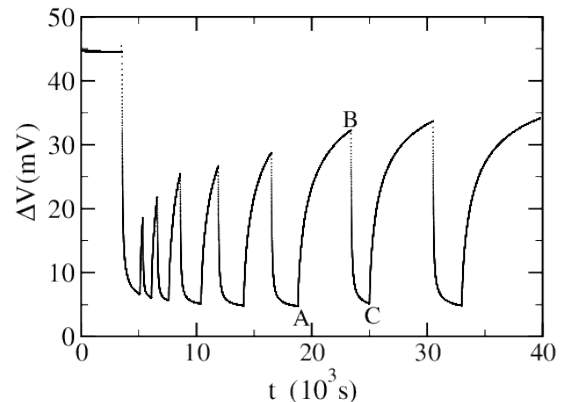

FIG. 8. Charging and discharging cycles of the TCC with Pt-foil electrodes, filled with 2 M EMIMTFSI in acetonitrile. Charging: curve AB. Discharging: curve BC. The time duration $(t_B - t_A)$ of charging is progressively increased. Discharging is made over a 20MΩ resistive load. Steady-state temperature difference is 20K. Heating is from the top electrode; heat flow is purely diffusive.
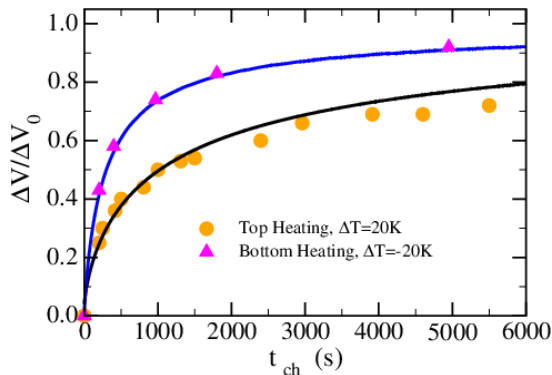
FIG. 9. Normalized charging potential $\Delta V/\Delta V_0$ as a function of time t_{ch}. Filled circles: Heating on the top electrode; pure diffusive heat flow. Filled triangles: Heating from the bottom electrode; convective heat flow. In both experiments, the steady-state temperature difference is 20 K. Full lines: Continuously time-recorded charging potential starting from a completely discharged cell and ending to the full charged state.

For pure EMIMTFSI using the current cell geometry and $\Delta T = 20$ K between the electrodes, $Ra \approx 20 \times 10^3$ well above the critical value. In our less viscous binary solution, this value is expected to be even higher. Consequently, heat transfer across the bottom and top electrodes is dominated by an almost turbulent convective heat flow rather than pure heat conduction through a stationary liquid.[39] It can be observed from Figure 9 that 50% of the fully charged state is achieved in $\Delta t \approx 250$ s when there are convective flows, whereas it takes ≈ 1000 s when the heat flow is purely diffusive. Clearly, convective flows accelerate the charging of the electric layer. In Figure 9 we have also plotted (full solid lines) the continuous differential voltage measurement during the (full) charging phase after completely discharging the TCC. Both curves (with and without convection) coincide remarkably well with the measurements performed in the charge/discharge sequence, showing the robustness of the electric layer charging process that can withstand many cycles.

III.4. Efficiency

The electrical energy stored at the IL/electrode interface and recovered through a single discharge is: $W = (1/2)C\Delta V^2 = (1/2)C\Lambda_{Pt}^2\Delta T^2$. With $\Lambda_{Pt} \approx -1.7$ mV/K at $\Delta T = 20^{o}$C, we obtain $W/A \approx 0.05$ mJ m^{-2}. During a charging time of $\Delta t \approx 250$ s (see section III.3.), the energy loss $\mathcal{Q}$ is essentially due to the heat flow from the hot to the cold electrode: $\mathcal{Q} \approx \kappa A\Delta t\Delta T/l$, where $\kappa \approx 0.3$ W m^{-1} K^{-1} is the thermal conductivity of the electrolyte and $l = 6$ mm the distance between electrodes.

The TCC efficiency is expressed by:

$$\eta = \frac{W}{\mathcal{Q}} = \frac{Tl\Lambda_{Pt}^2}{2\kappa\Delta t}\frac{C}{A}\eta_c \qquad (10)$$

where $\eta_c = \Delta T/T$ represents the Carnot efficiency. We obtain $\eta \approx 0.24 \times 10^{-9}\ \eta_c$, which is far too small for any imaginable waste-heat recovery application. However, the efficiency can be improved by adjusting various experimental parameters:

1. The electrode surface: Electrodes with larger effective surface area can be used to increase the specific capacity.

2. Thermoelectric coefficients: Λ of the order of 10 mV K^{-1} has been observed in solutions of tetraalkylammonium nitrate in alcohols.[40] Since the efficiency is proportional to Λ^2 a factor 100 might be gained by prospecting among the huge number of combinations IL/solvent.

3. The (re)charging time Δt can be shorter depending on the IL and the nature of the electrodes.

4. TCC geometry: The thermal heat loss may be substantially reduced by modifying the geometry of the cell (*e.g.* non uniform section with reduced diameter at mid distance between electrodes, or by intercalating a porous membrane between electrodes).

To illustrate, we have investigated one such example; namely the charging/discharging effect using nanoporous carbon electrodes, as presented in the following section.

IV. EXPERIMENTAL RESULTS WITH NANOPOROUS-CARBON ELECTRODES

A 0.2 mm thick and 4 mg weight nanoporous carbon (NanoTuneX Y-Carbon) electrode foil has been sandwiched between the platinum electrode and the cell body at both ends. N$_2$ adsorption/desorption isotherms were performed with a Micromeritics ASAP 2020 instrument. BET analysis gives a surface area of ≈ 300 m$^2/g$. The pore-size distribution is determined from desorption isotherm according to the BJH method. The average pore size is $\approx 20 \pm 10$ nm.

The thermoelectric coefficient under the same condition as in the previous section is $\Lambda_C = -0.3$ mV K^{-1}, approximately 6 times smaller than that obtained with Pt electrodes: $\Lambda_{Pt} = -1.7$ mV K^{-1}. This observation shows the importance of the interface potential $\phi(T)$ in Eq. (5) and its drastic dependence on the nature of the electrode. The remarkably large thermoelectic coefficient Λ on platinum electrodes is likely due to the configurational entropy change in EMIM$^+$ and/or TFSI$^-$ ions adsorbed at the surface.

A series of charging/discharging cycles through various resistive loads from 1.5 to 10 kΩ has been performed.

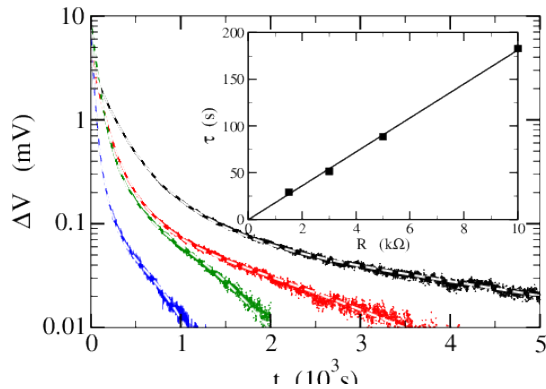FIG. 10. TCC with Y-Carbon electrodes. Discharge through different loads: 1.5 (blue), 3 (green), 5 (red), and 10 kΩ (black). The white dashed lines are fits through Eq. (9). The corresponding short relaxation times τ as a function of R are show in inset. The corresponding capacitance is 18.3 mF, four orders of magnitude larger than that obtained with Pt electrodes. Sample is 2M EMIMTFSI in acetonitrile.
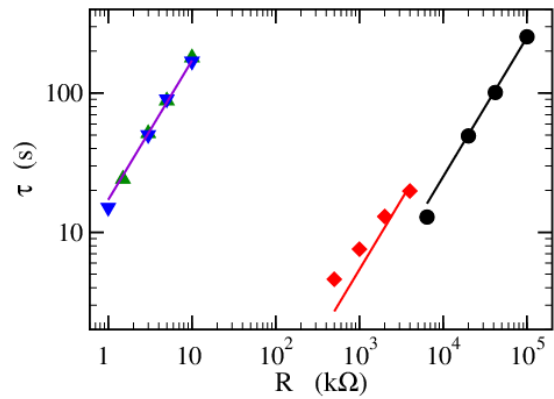

FIG. 11. Short charateristic times τ with: a) Two Pt electrodes (black circles); the black line corresponds to two capacitors with $C_{Pt} = 5$ μF in series; b) Two Y-Carbon nanoporous electrodes at 30–50°C (green up-triangles) and 30–70°C (blue down-triangles); the blue line corresponds to two capacitors with $C_C = 36.5$ mF in series; c) One Pt electrode and one Y-Carbon nanoporous electrode (red diamonds); the red line corresponds to two different capacitances $C_{Pt} = 5$ μF and $C_C = 36.5$ mF in series.

Note that, due to much larger capacitances of carbon electrodes, it was necessary to use much smaller R values here than those used with Pt electrodes.

The discharge potentials are shown in Figure 10. The results are fit once again to Eq. (9) to extract τ and θ. The corresponding short relaxation-times τ are reported in the inset, from which the differential capacitance of the system was determined as $C = 18.3$ mF, four orders of magnitude larger than that corresponding to Pt electrodes. The long time-scale constant $\theta \approx 2$ hours was obtained from $R = 10$ kΩ measurement; (note that for smaller R, the experimental time range ($t < \theta$) does not permit accurate determination of θ).

Applying a larger temperature difference $\Delta T = 40^oC$ with $T_{top} = 70^oC$ and $T_{bot} = 30^oC$ leads to the same conclusion. In Figure 11, the short characteristic times τ obtained using the two different ΔT values are compared. They lead to the same capacitance $C = 18.3$ mF. Therefore, by simply changing the electrode material, we were able to increase the TCC efficiency by $2 \approx 3$ orders of magnitude.

Finally, we have performed a set of charge/discharge with asymmetric electrodes: *i.e.*, nanoporous Y-Carbon electrode at the top, and Pt electrode at the bottom. The results are similar to those obtained with two symmetric pure platinum electrodes with a slightly higher capacitance value of 5.4 μF. The short characteristic times obtained under different measurement conditions are summarised in Figure 11. In all cases the cell can be modelled as two capacitances in series, taking $C_C = 36.5$ mF for a carbon electrode and $C_{Pt} = 5$ μF for a platinum electrode.

The specific capacitance for one carbon electrodes is $\approx 3\mu$F/cm^2, a value close to that deduced from Fig. 4 in Ref. 41: $\approx 4\mu$F/cm^2 from electrochemical analysis of

a 1 M solution of the ionic liquid tetraethylammonium tetrafluoroboride in acetonitrile.

V. CONCLUSION

We have investigated the thermal-to-electric energy conversion possibility in TCC's through charge accumulation in the electrical layers forming at the IL-electrode interface. The accumulated electric charge can be dissipated through an external load in a discontinuous way through a charge/discharge sequence while maintaining a steady-state temperature gradient across the cell. Most of the discharge occurs in a short time corresponding to a fast rearrangement of the IL/electrode interface. Repeated cycles of charge/discharge of the TCC show that the charging process is robust and well reproducible.

With no ionic electric current flowing through the cell, the described energy recovery process differs from that of most thermogalvanic cells. Some advantages of the present method include avoiding Joule heating and the reliance on the ionic conductivity, which tend to limit the efficiency of thermogalvanic cells.

Although the present efficiency value is not usable for any waste-heat recovery application, it can be improved greatly by a careful selection of electrode materials, ionic liquid and cell designs. Indeed, from Fig. 4 in Ref. 41, carbon nanopowder with higher surface area of order 2000 m^2/g increases the capacity by a factor 10 with respect to the presently used Y-Carbon. Other nanostructured electrodes, as nanoporous metals or carbon nanotubes can also be investigated. The charging time of the electric layer can also be reduced greatly by induc-

ing convective flows. Last but not the least a plethora of IL/electrode combinations can be explored to increase the thermoelectric coefficient Λ_e to maximize the voltage difference, and ultimately, to increase the efficiency of thermoelectric capacitors.

ACKNOWLEDGMENTS

[1] T. Kuroki, K. Kabeya, K. Makino, T. Kajihara, H. Kaibe, H. Hachiuma, H. Matsuno, and A. Fujibayashi, J. Electronic Materials **43**, 2405 (2014).

[2] B. Burrows, J. Electrochem. Soc. **123**, 154 (1976).

[3] J. Richter, Electrochimica Acta **22**, 1035 (1977).

[4] J. M. Hornut and A. Storck, J. Appl. Electrochem. **21**, 1103 (1991).

[5] Y. V. Kuzminskii, V. A. Zasukha, and G. Y. Kuzminskaya, J. of Power Sources **52**, 231 (1994).

[6] T. Hinoue, E. Ikeda, S. Watariguchi, and Y. Kibune, Anal. Chem. **79**, 291 (2007).

[7] A. Gunawan, C.-H. Lin, D. Buttry, A. V. Mujica, R. A. Taylor, R. S. Prasher, and P. E. Phelan, Nanoscale and Microscale Thermophysical Eng. **17**, 304 (2013).

[8] Y. Yamato, Y. Katayama, and T. Miura, J. Electrochemical Soc. **160**, H309 (2013).

[9] T. J. Abraham, D. R. MacFarlane, and J. M. Pringle, Energy Environ. Sci. **6**, 269 (2013).

[10] T. J. Abraham, D. R. MacFarlane, R. H. Baughman, L. Jin, N. Li, and J. M. Pringle, Electrochemica Acta **113**, 87 (2013).

[11] V. Zinovyeva, S. Nakamae, M. Bonetti, and M. Roger, ChemElectroChem **1**, 426 (2014).

[12] P. F. Salazar, S. Kumar, and B. A. B. A. Cola, J. Appl. Electrochem. **44**, 325 (2014).

[13] S. Uhl, E. Laux, T. Journot, L. Jeandupeux, J. Charmet, and H. Keppner, J. Electronic Materials **43**, 3758 (2014).

[14] T. I. Quickenden and Y. Mua, J. Electrochem. Soc. **142**, 3985 (1995).

[15] Y. Yang, S. W. Lee, H. Ghasemi, J. Loomis, X. Li, D. Kraemer, G. Zheng, Y. Cui, and G. Chen, Proc. Nat. Acad. Sci. **111**, 17011 (2014).

[16] M. Galinski, A. Lewandowski, and I. Stepniak, Electrochemica Acta **51**, 5567 (2006).

[17] N. S. Hudak and G. G. Amatucci, J. Electrochem. Soc. **158**, A572 (2011).

[18] Y. Qiao, V. K. Punyamurtual, A. Han, and H. Lim, J. Power Sources **183**, 403 (2008).

[19] B. Xu, L. Liu, H. Lim, Y. Qiao, and X. Chen, Nano Energy **1**, 805 (2012).

[20] H. Lim, W. Lu, and Y. Qiao, Appl. Phys. Lett. **101**, 063902 (2012).

[21] H. Lim, W. Lu, X. Chen, and Y. Qiao, Nanotechnology **24**, 465401 (2013).

[22] J. Agar, *Thermogalvanic cells* (Paul Delahay ed., Interscience New York, 1963) Chap. Advances in Electrochemistry and Electrochemical Engineering, pp. 31 – 121.

[23] H. L. Ngo, K. LeCompte, L. Hargens, and A. B. McEwen, Thermochemica Acta **357-358**, 97 (2000).

[24] M. Hayyan, F. S. Mjalli, M. A. Hashim, I. M. AlNashef, and T. X. Mei, J. Ind Eng. Chem. **19**, 106 (2013).

[25] Y. Z. Su, Y. C. Fu, Y. M. Wei, J. W. Yan, and B. W. Mao, ChemPhysChem **11**, 2764 (2010).

[26] Y. Z. Su, Y. C. Fu, J. W. Yan, Z. B. Chen, and B. W. Mao, Angew. Chem. Int. Ed. **48**, 5148 (2009).

[27] A. B. McEwen, H. L. Ngo, K. LeCompte, and J. L. Goldman, J. Electrochemical Soc. **146**, 1687 (1999).

[28] G. B. Pan and W. Freyland, Chem. Phys. Lett. **427**, 96 (2006).

[29] D. Wakeham, R. Hayes, G. G. Warr, and R. Atkin, J. Phys. Chem. B **113**, 5961 (2009).

[30] T. Cremer, M. Stark, A. Deyko, S. H. P., and F. Maier, Langmuir **27**, 3662 (2011).

[31] F. Silva, C. Gomes, M. Figueiredo, R. Costa, A. Martins, and C. M. Pereira, J. Electroanal. Chem. **662**, 153 (2008).

[32] V. Lockett, R. Sedev, J. Ralston, M. Horne, and T. Rodopoulos, J. Phys. Chem. C **112**, 7486 (2008).

[33] A. Würger, Phys. Rev. Lett. **101**, 108302 (2008).

[34] J. A. Bierlein, J. Chem. Phys. **23**, 10 (1955).

[35] J. N. Agar and J. C. R. Turner, Proc. Royal Soc. London **A 225**, 307 (1959).

[36] A. Noda, K. Hayamizu, and W. Watanabe, J. Phys. Chem. B **105**, 4603 (2001).

[37] V. V. Chaban, I. V. Voroshylova, O. N. Kalugin, and O. V. Prezhdo, J. Phys. Chem. B **116**, 7719 (2012).

[38] D. M., B. Huber, and B. Roling, J. Phys. Chem. C **115**, 6802 (2011).

[39] P. G. Drazin and W. H. Reid, *Hydrodynamic Stability* (Cambridge University Press, Cambridge, 1981).

[40] M. Bonetti, S. Nakamae, M. Roger, and P. Guenoun, J. Chem. Phys. **134**, 114513 (2011).

[41] O. Barbieri, M. Hahn, A. Herzog, and R. Kötz, Carbon **43**, 1303 (2005).